

Comparison of PACS-*Scanamorphos* and MIPS surface brightnesses for diffuse and very extended emission

H. Roussel

Institut d'Astrophysique de Paris, Université Pierre et Marie Curie (UPMC), CNRS (UMR 7095), 75014 Paris, France
e-mail: roussel@iap.fr

software webpage: <http://www2.iap.fr/users/roussel/herschel/>

This short document was made in response to the 6th referee report on the ill-fated *Scanamorphos* paper (arXiv:1205.2576). It refutes the claim made in this referee report that any software exploiting the redundancy to subtract low-frequency noise necessarily filters out emission that is more extended than the array, and takes a new look at the conservation of diffuse and very extended emission in maps made with *Scanamorphos*. It is very difficult to make realistic simulations for diffuse emission, because the staring observations that are used as low-frequency noise input are affected by strong digitization noise that is higher than in real observations, making them useable only for bright fields. Therefore, real observations are compared with a reference taken from another instrument not suffering from low-frequency noise.

1. Preamble

This document complements similar studies already carried out by PACS ICC members for the latest Herschel map-making workshop (ESAC, January 2013). It focuses more on very diffuse emission, to comply with the referee's demands. The analysis is restricted to PACS data, since the SPIRE instrument is much less affected by low-frequency noise and is less prone to processing artefacts. The ancillary data that are suitable for a comparison with PACS are limited. IRAS (or IRIS) data are not directly useable because the uncertainties on the spatially-variable gain (of the order of 15%) and on the PSF (also spatially variable, elliptical and not characterized in any detail) are too large, and the angular resolutions of IRAS and PACS are too dissimilar (see Ali 2013). Spitzer-MIPS data are better suited, since the flux calibration accuracy is higher, and one does not have to worry too much about low-frequency noise. Non-linearities affect the MIPS arrays, but start at brightnesses above 50 to 100 MJy/sr (see references in Paladini 2013). The angular resolution conversion is under control, using the convolution kernels computed by Aniano et al. (2011). For this comparison, cirrus fields are taken from the Herschel Gould belt survey (HGBS), a large key project (André et al. 2010). They are chosen by inspecting the archive images, among fields that are not larger than ~ 2 square degrees and among the faintest fields (very little structure visible at $160\ \mu\text{m}$ and none at $70\ \mu\text{m}$, with the automatic pipeline processing).

2. L1241

This field of 2.2 square degrees is one of the most diffuse fields in the HGBS and is part of the Spitzer program "Gould's Belt: Star Formation in the Solar Neighborhood" (P.I. Lori Allen). The PACS observations with Herschel were made at 100 and $160\ \mu\text{m}$ in nominal mode, and 70 and $160\ \mu\text{m}$ in parallel mode. When I started this analysis, I did not look at the parallel-mode program, so I took the $160\ \mu\text{m}$ data from the nominal mode observations.

PACS₇₀: obsids 1342188679 and 1342188680 (2 scans)

PACS₁₆₀: obsids 1342197673 and 1342197674 (2 scans)

MIPS: obsids r19964416 and r19964928

At $160\ \mu\text{m}$, MIPS BCD data (the equivalent of level-1 data for Herschel) are downloaded from the Spitzer Heritage Archive (SHA). There are 2303 BCDs in prime time. The readouts that are affected by stim-flash latents are first detected and masked out. Then the mosaic is built with Mopex (Makovoz et al. 2006), using the default pixel size of $16''$. At $70\ \mu\text{m}$, MIPS BCD data are also retrieved from the SHA (2400 BCDs in prime time). Bad frames are masked out and the data are flat-fielded before being combined into a mosaic with Mopex (pixel size of $5.6''$, i.e. 4 times the pixel size of the PACS map).

The PACS signal and error maps reduced with *Scanamorphos* are convolved to the angular resolution of MIPS (after masking out the edges of the maps with a weight that is below 0.4 times the median weight), and rebinned to obtain the same pixel grid as MIPS. The astrometry of the MIPS map is then matched to that of the PACS map by using the IDL Astronomy User's Library routine *hastrom*. I recall that since PACS is not an absolute photometer, the zero-order brightness in PACS maps is arbitrary. The median

offset between the PACS and MIPS maps is therefore cancelled before comparing the surface brightnesses.

Following Paladini (2013), the following color corrections, appropriate for $T = 20$ K dust, are applied to account for the different filter transmission curves:

$$PACS_{70\text{ corr}} = PACS_{70\text{ mes}} / 1.224 \times 1.153 \quad \text{and} \quad MIPS_{70\text{ corr}} = MIPS_{70\text{ mes}} / 1.052$$
$$PACS_{160\text{ corr}} = PACS_{160\text{ mes}} / 0.963 \times 0.959 \quad \text{and} \quad MIPS_{160\text{ corr}} = MIPS_{160\text{ mes}} / 0.944$$

The results are presented below (Fig. 1 to 4 and 13). At $160\mu\text{m}$, the least-absolute-deviation fit shown in Fig.13 is $PACS_{160} = -1.22 + 1.02 MIPS_{160}$. If the color corrections are not applied, the best-fit slope changes from 1.02 to 1.09.

At $70\mu\text{m}$, the least-absolute-deviation fit is meaningless, since there is only a cloud of points with no obvious correlation. There are two causes: 1) The MIPS map suffers from severe artefacts, and the uncertainty map produced by Mopex vastly underestimates the errors. 2) At $70\mu\text{m}$, the high-frequency noise in PACS data is completely dominated by strong digitization noise, and the signal is not significant (see the signal-to-noise ratio map).

3. Lupus IV

This field of 1.5 square degree, a target of the HGBS too, is part of the Spitzer program “From molecular cores to planets” (P.I. Neal Evans). As for L1241, the $160\mu\text{m}$ data are taken from nominal-mode observations, and the $70\mu\text{m}$ data from parallel-mode observations. The processing and analysis are made in the same way as described above. There are 2129 prime BCDs from $MIPS_{160}$ and 2000 for $MIPS_{70}$.

PACS₇₀: obsids 1342203087 and 1342203088 (2 scans)
PACS₁₆₀: obsids 1342228968 and 1342228969 (2 scans)
MIPS: obsids r5730304 and r5730560

The results are presented below (Fig.5 to 8 and 14). At $160\mu\text{m}$, the least-absolute-deviation fit shown in Fig.14 is $PACS_{160} = -6.59 + 1.07 MIPS_{160}$. If the color corrections are not applied, the best-fit slope changes from 1.07 to 1.13.

At $70\mu\text{m}$, the least-absolute-deviation fit (Fig.14) is $PACS_{70} = 0.08 + 1.00 MIPS_{70}$, and the slope changes by less than 1% if the color corrections are not applied. However, the correlation appears to be mostly driven by compact sources, and the diffuse underlying emission is too faint to yield significant results. This is obvious by looking at the PACS signal-to-noise ratio map: because the high-frequency noise is completely dominated by strong digitization noise, the signal is not significant. It can nevertheless be noted that diffuse emission looks very similar in both maps.

4. L1712

In order to deal with more significant emission at $70\mu\text{m}$, I next hunted for brighter fields than L1241 and Lupus IV with MIPS counterparts. L1712 (2.6 square degrees) is part of the HGBS and the same Spitzer program as Lupus IV. The processing and analysis are made in the same way as described above, except that to distinguish latent frames from valid frames in MIPS data requires great care. There are 6505 prime BCDs for $MIPS_{70}$. The analysis is not made at $160\mu\text{m}$ since the signal-to-noise ratio is higher than wanted, and non-linearity effects can be expected to be severe in MIPS data.

PACS₇₀: obsids 1342204088 and 1342204089 (2 scans)
MIPS: obsids r5748992, r5749248, r5749504, r5753344, r5753600 and r5753856

The results are presented below (Fig.9, 10 and 15). The least-absolute-deviation fit shown in Fig.15 is $PACS_{70} = 1.33 + 0.97 MIPS_{70}$. Restricting the fit to points below 110 MJy/sr in both maps (i.e. excluding compact sources), the slope becomes 1.00 instead of 0.97.

5. Per02

Since the HGBS diffuse fields of moderate size are all very faint at $70\mu\text{m}$, I next chose a field containing locally bright emission, Per02, of 8 square degrees (in the same Spitzer program as Lupus IV and L1712). There are 9169 prime BCDs for $MIPS_{70}$. The processing and analysis are the same as for L1712.

PACS₇₀: obsids 1342214504 and 1342214505 (2 scans)
MIPS: obsids r5780992, r5781248, r5781504, r5781760, r5782016, r5787648, r5787904, r5788160, r5788416 and r5788672

The results are presented below (Fig. 11, 12 and 16). The least-absolute-deviation fit shown in Fig. 16, using all data including those affected by strong non-linearities, is $PACS_{70} = -15.50 + 1.55 MIPS_{70}$. Restricting the data to points below 200 MJy/sr in the average of both maps, the fit becomes $PACS_{70} = -0.73 + 1.03 MIPS_{70}$.

6. Conclusion

At $160\ \mu\text{m}$, the extended diffuse emission is recovered accurately, with deviations from the MIPS reference map that are much smaller than the photometric uncertainties. A slight non-linearity is present at high surface brightness (PACS brightnesses being greater than MIPS brightnesses), which is a known feature of MIPS (Paladini 2013), not corrected for in the automatic pipeline. The Lupus IV field has localized emission that is brighter than in L1241, which explains that non-linearity effects are more severe for this field. Excluding these regions, the difference map shows that deviations between PACS and MIPS are not spatially structured like real emission, and are much smaller than the photometric uncertainties. Localized deviations of the order of 1σ can easily be explained by obvious artefacts of the MIPS maps.

At $70\ \mu\text{m}$, the PACS maps contain diffuse emission with credible distribution, but its brightness above background is well below the 3σ significance level (except for parts of the map of Per02), because the observational setup, with high quantization noise, is not suited to the detection of very faint signals. The comparison with MIPS is inconclusive for L1241 and Lupus IV. For L1712, which is brighter, the diffuse emission is in very good agreement in MIPS and PACS maps, despite the fact that the emission is everywhere below the 3σ level in PACS data. The low quality of the MIPS map, with clear stripes along the scan direction, can explain some of the artefacts in the difference map. For Per02, which is still brighter, the diffuse emission is again in very good agreement in MIPS and PACS maps, excluding the brighter areas affected by strong non-linearities in MIPS data. For this field too, some clear artefacts are present in the MIPS map (stripes and offsets between sub-fields), which unfortunately limits the degree to which the pixel-per-pixel comparison can be interpreted.

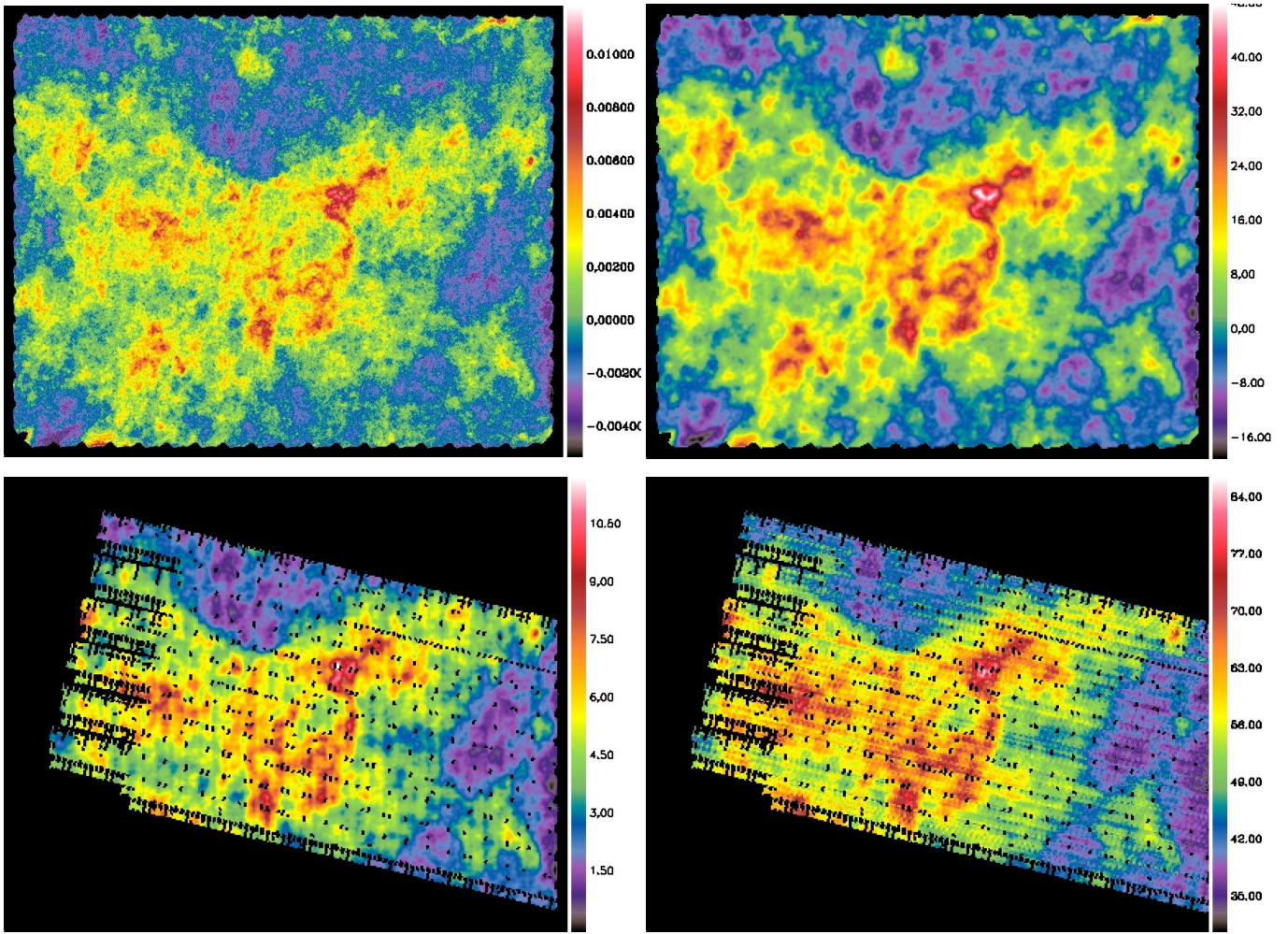


Fig. 1. L1241

Top left: Initial PACS₁₆₀ map in Jy/pixel, with 2.85'' pixels (FWHM/4).

Top right: PACS₁₆₀ map in MJy/sr after convolution the MIPS₁₆₀ angular resolution and rebinning on 16'' pixels.

Bottom left: PACS₁₆₀ signal-to-noise ratio map, on the MIPS grid.

Bottom right: MIPS₁₆₀ map in MJy/sr, with 16'' pixels, matched to the astrometry of the PACS map.

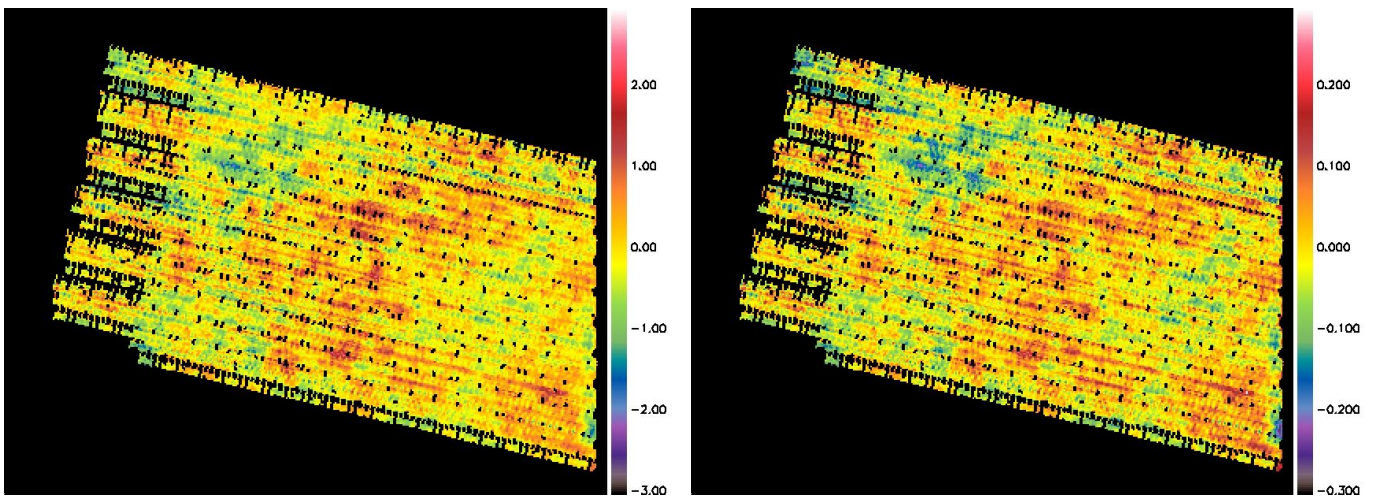


Fig. 2. L1241

Left: PACS₁₆₀ - MIPS₁₆₀ difference, normalized by the photometric uncertainty (displayed range: -3σ to $+3\sigma$).

Right: PACS₁₆₀ - MIPS₁₆₀ difference, normalized by the MIPS₁₆₀ map (displayed range: -30% to $+30\%$).

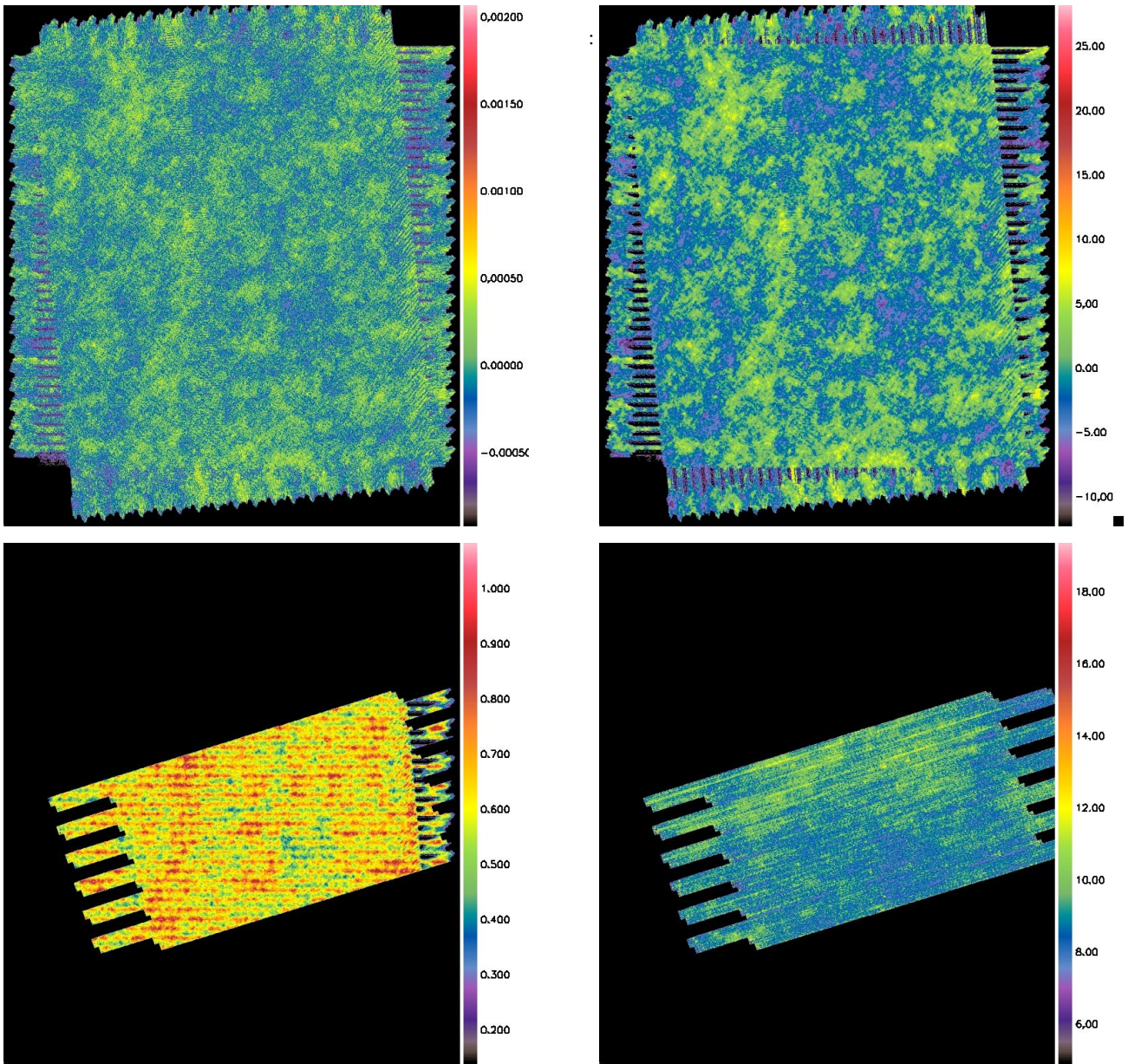


Fig. 3. L1241

Top left: Initial PACS₇₀ map in Jy/pixel, with 1.4'' pixels (FWHM/4).

Top right: PACS₇₀ map in MJy/sr after convolution the MIPS₇₀ angular resolution and rebinning on 5.6'' pixels.

Bottom left: PACS₇₀ signal-to-noise ratio map, on the MIPS grid.

Bottom right: MIPS₇₀ map in MJy/sr, with 5.6'' pixels, matched to the astrometry of the PACS map.

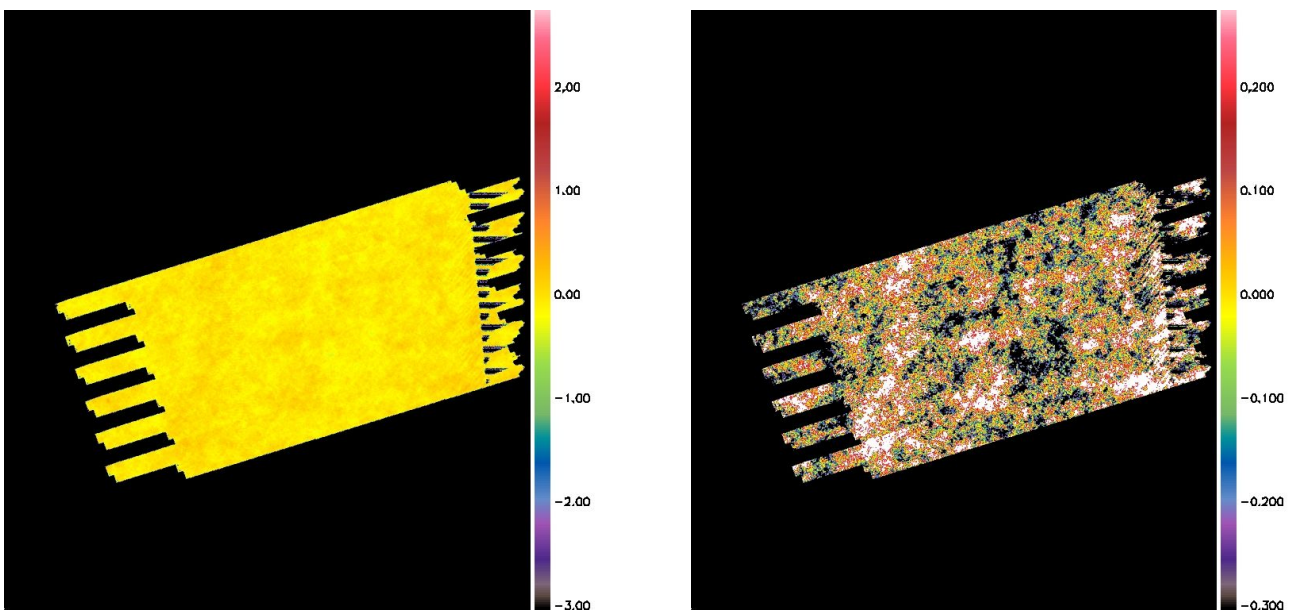


Fig. 4. L1241

Left: PACS₇₀ - MIPS₇₀ difference, normalized by the photometric uncertainty (displayed range: -3σ to $+3\sigma$).

Right: PACS₇₀ - MIPS₇₀ difference, normalized by the MIPS₇₀ map (displayed range: -30% to $+30\%$).

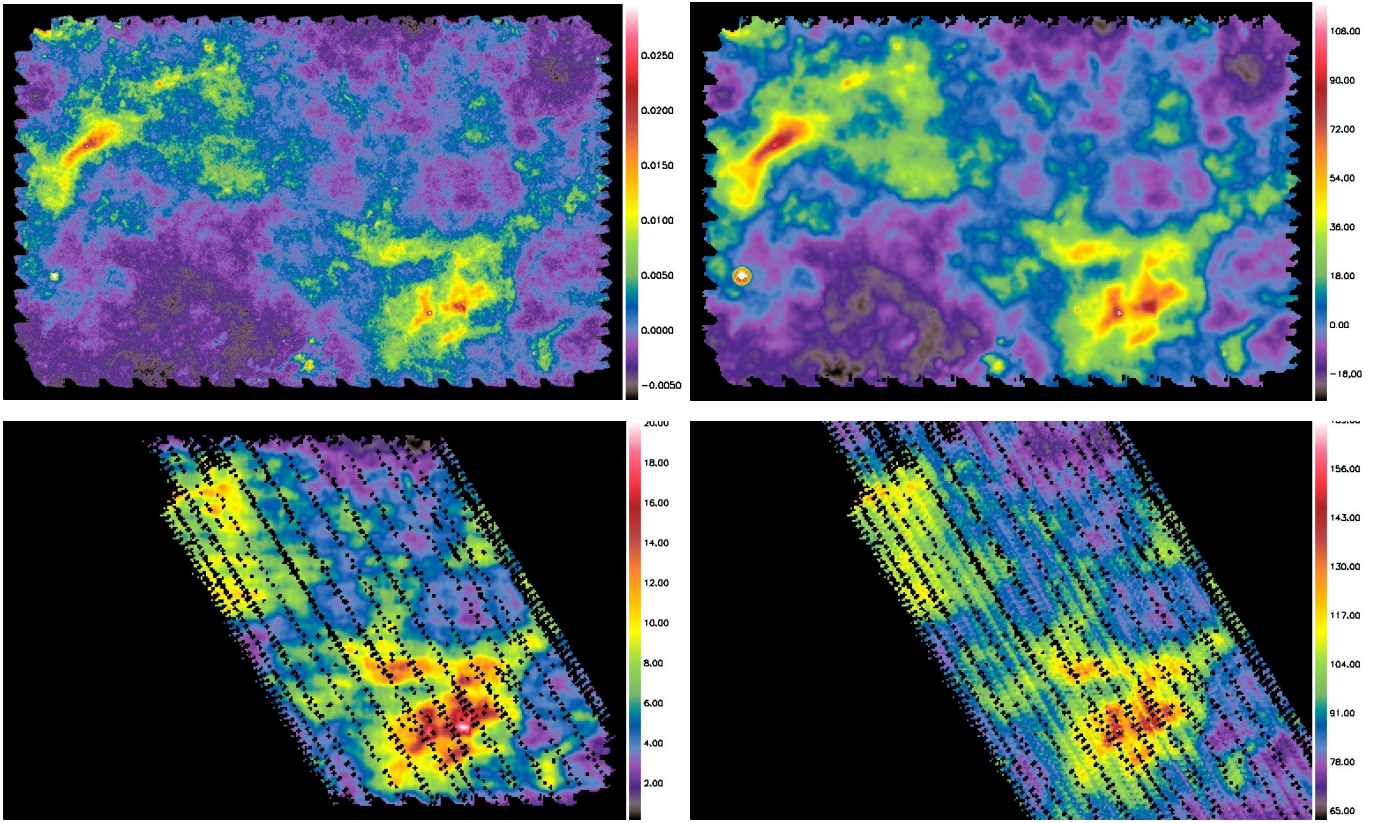


Fig. 5. Lupus IV

Top left: Initial PACS₁₆₀ map in Jy/pixel, with 2.85'' pixels (FWHM/4).

Top right: PACS₁₆₀ map in MJy/sr after convolution the MIPS₁₆₀ angular resolution and rebinning on 16'' pixels.

Bottom left: PACS₁₆₀ signal-to-noise ratio map, on the MIPS grid.

Bottom right: MIPS₁₆₀ map in MJy/sr, with 16'' pixels, matched to the astrometry of the PACS map.

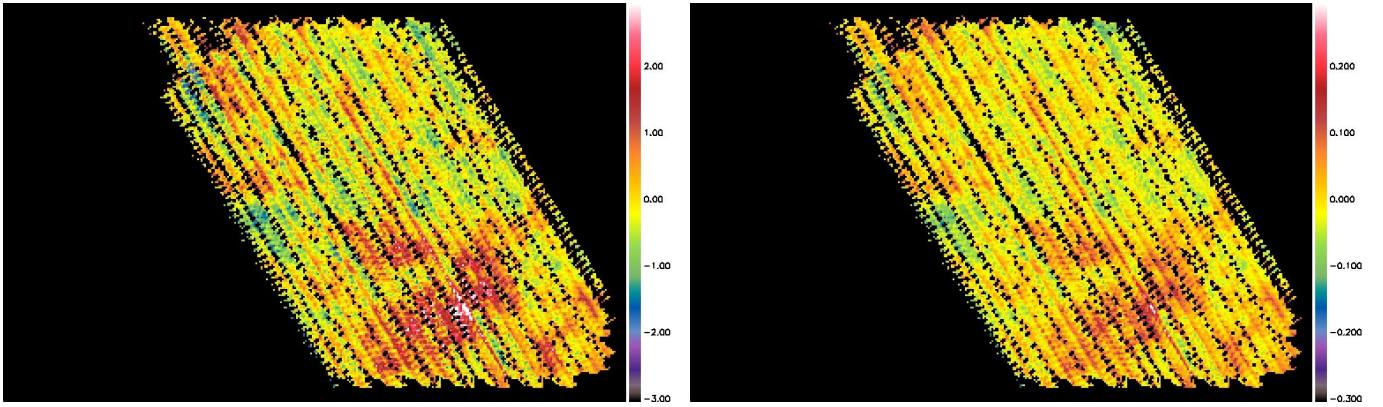


Fig. 6. Lupus IV

Left: PACS₁₆₀ - MIPS₁₆₀ difference, normalized by the photometric uncertainty (displayed range: -3σ to $+3\sigma$).

Right: PACS₁₆₀ - MIPS₁₆₀ difference, normalized by the MIPS₁₆₀ map (displayed range: -30% to $+30\%$).

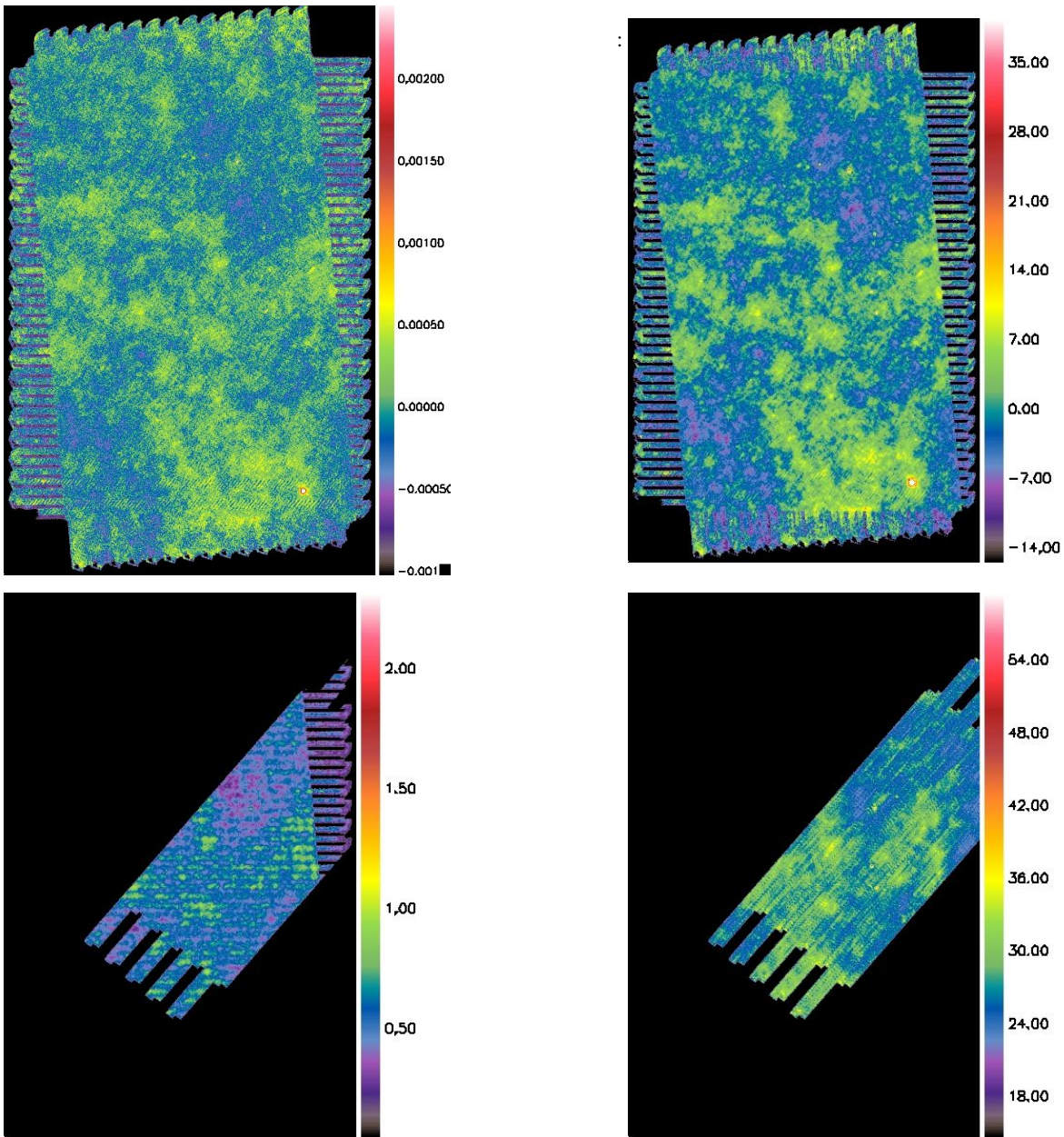


Fig. 7. Lupus IV

Top left: Initial PACS₇₀ map in Jy/pixel, with 1.4'' pixels (FWHM/4).

Top right: PACS₇₀ map in MJy/sr after convolution the MIPS₇₀ angular resolution and rebinning on 5.6'' pixels.

Bottom left: PACS₇₀ signal-to-noise ratio map, on the MIPS grid.

Bottom right: MIPS₇₀ map in MJy/sr, with 5.6'' pixels, matched to the astrometry of the PACS map.

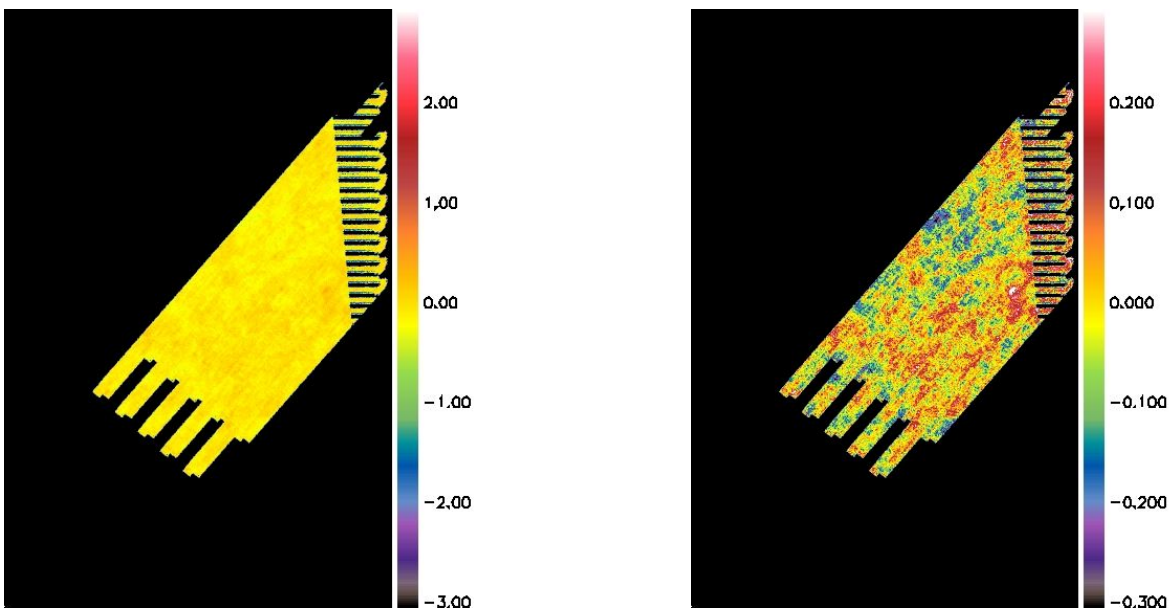


Fig. 8. Lupus IV

Left: PACS₇₀ - MIPS₇₀ difference, normalized by the photometric uncertainty (displayed range: -3σ to $+3\sigma$).

Right: PACS₇₀ - MIPS₇₀ difference, normalized by the MIPS₇₀ map (displayed range: -30% to $+30\%$).

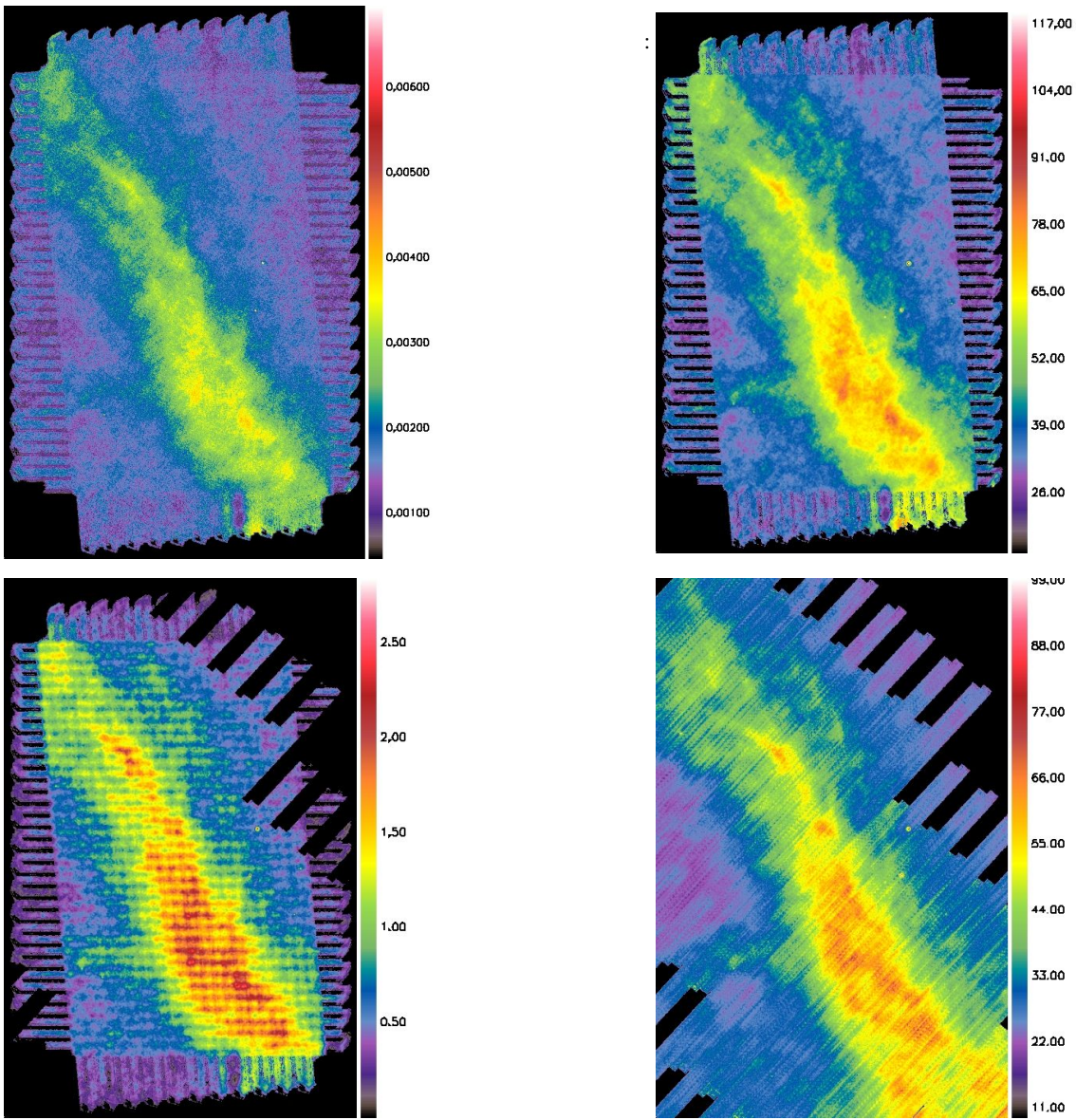


Fig. 9. L1712

Top left: Initial PACS₇₀ map in Jy/pixel, with 1.4'' pixels (FWHM/4).

Top right: PACS₇₀ map in MJy/sr after convolution the MIPS₇₀ angular resolution and rebinning on 5.6'' pixels.

Bottom left: PACS₇₀ signal-to-noise ratio map, on the MIPS grid.

Bottom right: MIPS₇₀ map in MJy/sr, with 5.6'' pixels, matched to the astrometry of the PACS map.

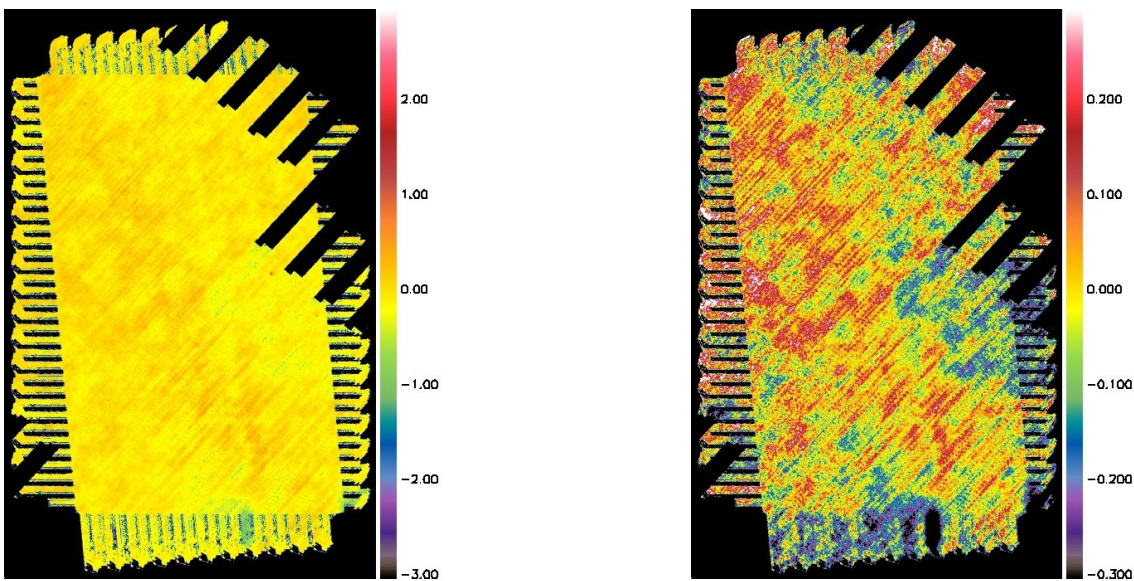


Fig. 10. L1712

Left: PACS₇₀ - MIPS₇₀ difference, normalized by the photometric uncertainty (displayed range: -3σ to $+3\sigma$).

Right: PACS₇₀ - MIPS₇₀ difference, normalized by the MIPS₇₀ map (displayed range: -30% to $+30\%$).

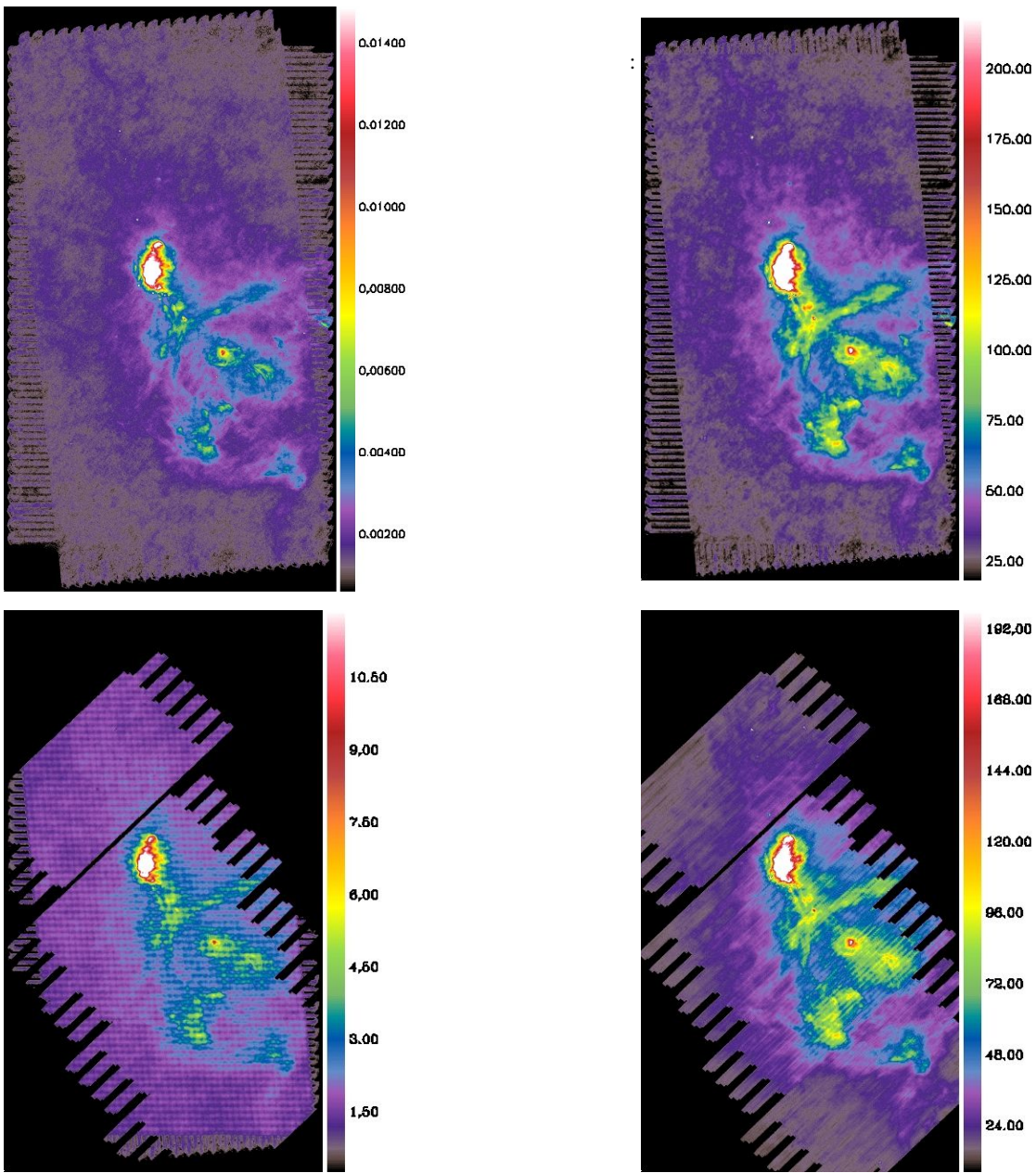


Fig. 11. Per02

Top left: Initial PACS₇₀ map in Jy/pixel, with 1.4'' pixels (FWHM/4).

Top right: PACS₇₀ map in MJy/sr after convolution the MIPS₇₀ angular resolution and rebinning on 5.6'' pixels.

Bottom left: PACS₇₀ signal-to-noise ratio map, on the MIPS grid.

Bottom right: MIPS₇₀ map in MJy/sr, with 5.6'' pixels, matched to the astrometry of the PACS map.

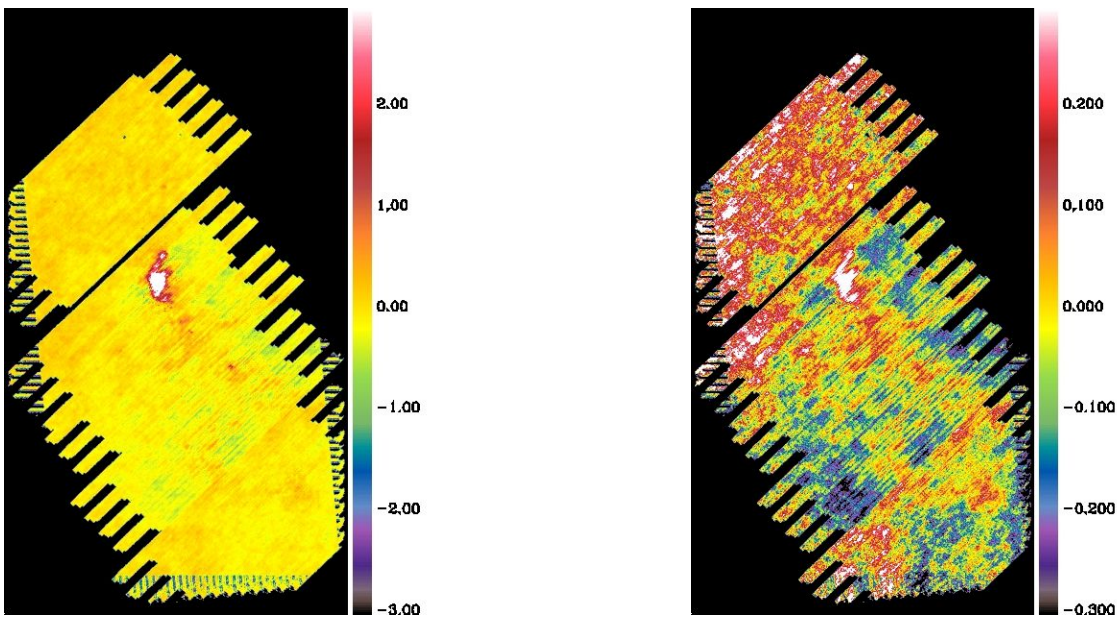


Fig. 12. Per02

Left: PACS₇₀ - MIPS₇₀ difference, normalized by the photometric uncertainty (displayed range: -3σ to $+3\sigma$).

Right: PACS₇₀ - MIPS₇₀ difference, normalized by the MIPS₇₀ map (displayed range: -30% to $+30\%$).

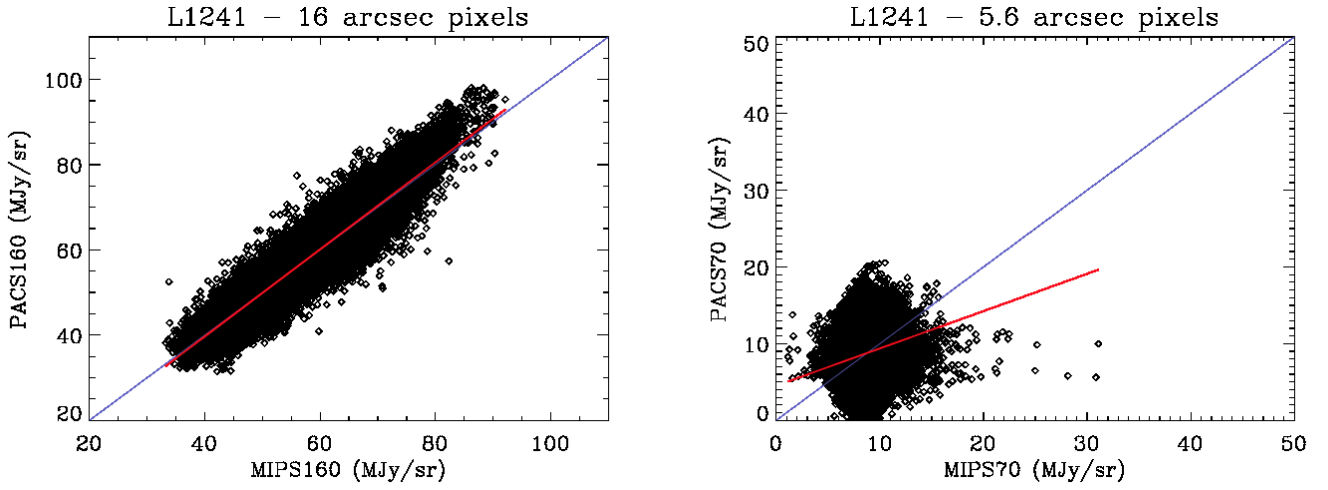


Fig. 13. L1241: pixel-to-pixel comparison of surface brightnesses from MIPS (abscissa) and PACS (ordinate), at $160\ \mu\text{m}$ (left) and $70\ \mu\text{m}$ (right). The blue line is the linear relation, and the red line is the best least-absolute-deviation fit.

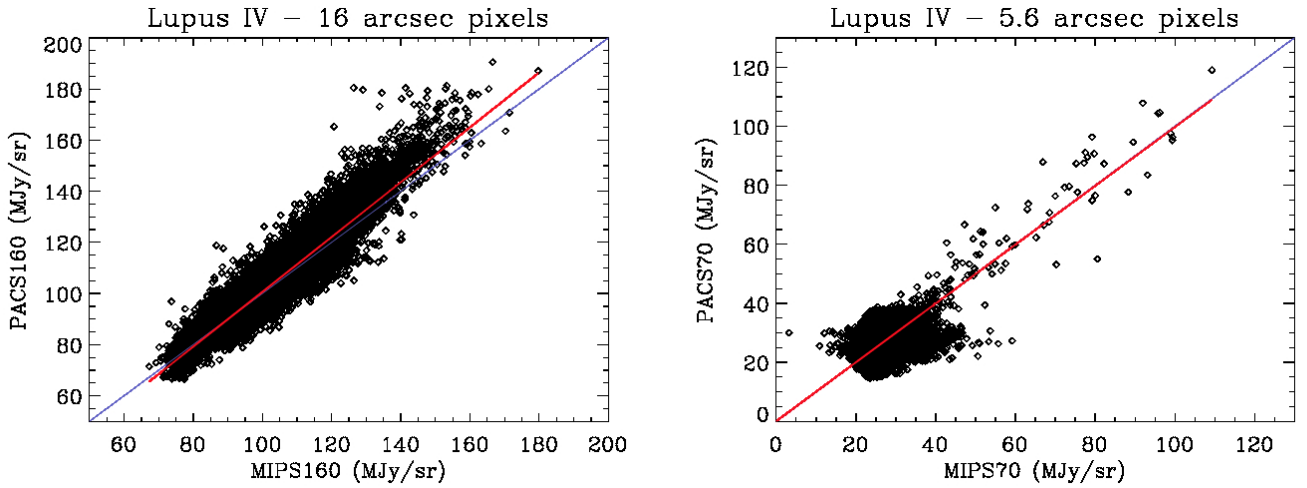


Fig. 14. Lupus IV: pixel-to-pixel comparison of surface brightnesses from MIPS (abscissa) and PACS (ordinate), at $160\ \mu\text{m}$ (left) and $70\ \mu\text{m}$ (right). The blue line is the linear relation, and the red line is the best least-absolute-deviation fit.

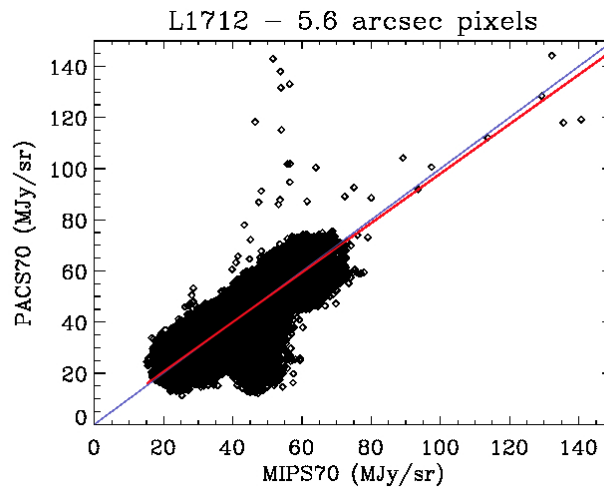


Fig. 15. L1712: pixel-to-pixel comparison of surface brightnesses from MIPS (abscissa) and PACS (ordinate) at $70\ \mu\text{m}$. The blue line is the linear relation, and the red line is the best least-absolute-deviation fit using all points (a few of which go above the displayed maximum).

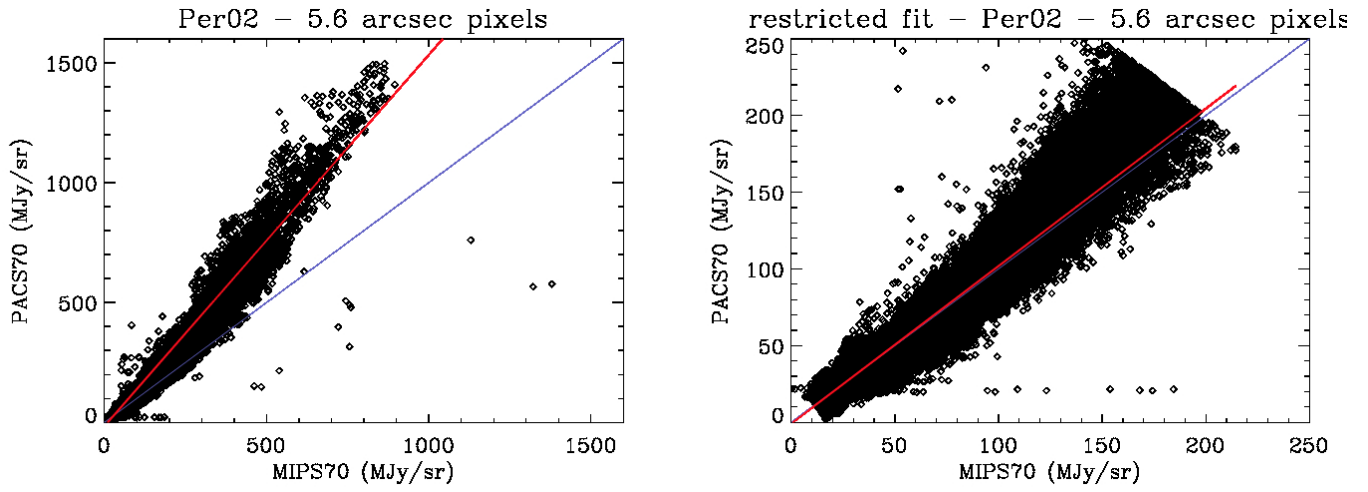


Fig. 16. Per02: pixel-to-pixel comparison of surface brightnesses from MIPS (abscissa) and PACS (ordinate) at $70\ \mu\text{m}$. The blue line is the linear relation, and the red line is the best least-absolute-deviation fit using all points (left) and using points below $200\ \text{MJy/sr}$ in the average of both maps (right).

References

- Ali, B. 2013, "PACS-IRAS comparison at $100\ \mu\text{m}$ ", Herschel map-making workshop, ESAC, January 2013
 André, P., Men'shchikov, A., Bontemps, S., et al. 2010, *A&A*, 518, L102
 Aniano, G, Draine, B.T., Gordon, K.D., & Sandstrom, K. 2011, *PASP*, 123, 1218
 Makovoz, D., Khan, I., & Masci, F. 2006, *SPIE*, 6065, 330
 Paladini R. 2013, "PACS benchmarking: comparison with Spitzer MIPS", Herschel map-making workshop, ESAC, January 2013